Heat partitioning in terrestrial planets during core formation by negative diapirism

H. Samuel [a,*], P.J. Tackley [b], M. Evonuk [c]

[a] *Bayerisches Geoinstitut, Universität Bayreuth, Germany*
[b] *Department of Geophysical Fluid Dynamics, ETH Zürich, Switzerland*
[c] *Department of Theoretical Physics I, Universität Bayreuth, Germany*

ARTICLE INFO

ABSTRACT

We investigate the gravitational heat partitioning between silicate and metallic phases during core formation by negative diapirism in terrestrial planets. We model the dynamic evolution of an iron diapir, sinking through a solid silicate proto-mantle. Our calculations include viscous heating and strong temperature and composition-dependence of viscosity. We show that the diapir mean temperature evolves towards an asymptotic value $T_{d\infty}$, which depends on the efficiency of viscous heating and heat transfer between the diapir and its surroundings, and on the viscous rheology. We derived a simple analytic model that captures the thermal evolution observed in our numerical experiments. This model can be applied to determine the heat distribution within terrestrial planets with a large number of diapirs, during their growth and early differentiation. We show that the partitioning of core formation heating during negative diapirism depends strongly on the size distribution of the iron diapirs. A large number of small sinking iron diapirs favors metal–silicate heat exchange and leads to a relatively hot core, which allows a sustainable dynamo, as on Earth. A small number of large diapirs have the opposite effect and could correspond to a Mars-like planet with an early dynamo that is no longer active. In all cases, negative diapirism tends to leave the lowermost mantle significantly hotter than its upper part, which could trigger large amounts of melting in the early deep mantle.

1. Introduction

Core formation is the first major differentiation event that determines the initial conditions from which the Earth and other terrestrial planets have evolved. The separation of metal and silicate in terrestrial planets is likely to generate ~10^{29} to 10^{31} J of heat for Mars- to Earth-like planets by conversion of potential into thermal energy via viscous heating (Rubie et al., 2007; Solomon, 1979). This represents a temperature increase of few hundreds to few thousands of Kelvin depending on its partitioning.

While estimating the total amount of gravitational heating in a planet is relatively straightforward, determining its partitioning between the silicate and metallic part is not a trivial task and depends on the segregation mechanism. Negative diapirism is one plausible core formation scenario in which metal diapirs sink through a lighter proto-mantle (Karato and Murthy, 1997; Rubie et al., 2007; Stevenson, 1981; Tonks and Melosh, 1992). Recently, the dynamics of core formation scenarios have been studied by means of numerical experiments (Golabek et al., 2008; Monteux et al., 2009; Ricard et al., 2009; Samuel and Tackley, 2008), and laboratory experiments (Olson and Weeraratne, 2008). However, the question of gravitational/viscous heat partitioning for sinking diapirs with a strong thermally and compositionally dependent rheology has so far not been addressed. Consequently, studies that have investigated the thermal evolution and differentiation of growing terrestrial planets by negative diapirism have assumed an arbitrary heat partitioning between the sinking diapirs and their surroundings (Sasaki and Nakazawa, 1986; Senshu et al., 2002).

We thus investigate dynamically the heat partitioning between metal and silicate during core formation by negative diapirism using numerical modeling. We then derive general scaling laws for the time evolution of heat distribution between the iron diapirs and the silicate material and use them to determine the heat distribution within terrestrial planets during their growth and early differentiation.

2. Dynamical and thermal evolution

We first study numerically the heat partitioning between a metal diapir sinking through a silicate mantle by monitoring its thermal evolution. We subsequently propose simpler models that describe the thermal evolution we observe in our numerical experiments.

2.1. Numerical experiments

The governing equations and the numerical setup are identical to Samuel and Tackley, (2008) and will only be briefly summarized here. Using a finite volume code (Tackley, 2008) in spherical axisymmetric

---

geometry, we solve for the conservation of mass, momentum, energy and composition, under the extended Boussinesq approximation and in the limit of infinite Prandtl number. The model assumes constant gravity g. Density varies as $\rho = \rho_0 (1 - \alpha\, T'\Delta T) + C\Delta\rho_c$, where ρ_0 is the reference silicates density, α is the thermal expansion, T' the dimensionless potential excess temperature, ΔT a characteristic temperature scale, $\Delta\rho_c$ is the metal to silicate density contrast, and C is the composition that ranges from 0 (pure silicate) to 1 (pure metal). Viscosity varies according to $\eta(T', C) = \eta_0 \exp(-T' \ln\gamma)/[1 + C\,(10^3 - 1)]$. This law accounts for a sharp compositional viscosity decrease of three orders of magnitude in the iron material, which is large enough to consider $\eta_{\text{Diapir}} \ll \eta_{\text{Silicates}}$. The parameter γ represents the sensitivity of viscosity to temperature. Apart from density and viscosity, all the physical parameters have no dependence in C. Since we consider cases where compositional density contrasts largely dominate over the thermal density contrasts ($\rho \cong \rho_0 + C\Delta\rho_c$), the system evolves towards a steady state solution for both temperature and flow. The diapir reaches a terminal sinking velocity V_s, as long as it remains far from the closed boundaries (Samuel and Tackley, 2008).

By non-dimensionalizing the governing equations using the diapir's radius r_d for distance, ρ_0 for density, η_0 for viscosity, ΔT for temperature, and V_s for velocity, conservation of the energy is written:

$$\frac{\partial T'}{\partial t'} + \mathbf{U}'.\nabla T' = \frac{1}{P_e} \nabla^2 T' + \Pi_v(\phi_v' - T' U_r'), \tag{1}$$

where t is time, $\mathbf{U} = (U_r, U_\theta)$ is the velocity vector and ϕ_v is the viscous dissipation function. Primes denote dimensionless variables. The last two terms on the right hand side of Eq. (1) are respectively the production of heat due to the conversion of gravitational potential energy into thermal energy, and the contribution of adiabatic heating/cooling. The later is negligible compared to viscous heating. The first dimensionless number in Eq. (1) is a diapir thermal Péclet number:

$$P_e = \frac{V_s r_d \rho_0 C_p}{k}, \tag{2}$$

where k the thermal conductivity and C_p the specific heat at constant pressure. As P_e increases, diffusive heat transfer between the diapir and its surrounding becomes less efficient. The second number expresses the efficiency of viscous heating:

$$\Pi_v = \frac{V_s \eta_0}{r_d \Delta T \rho_0 C_p}. \tag{3}$$

As Π_v increases, the temperature increase due to viscous heating becomes more important.

The dimensionless numbers P_e, Π_v and the rheological parameter γ, represent the governing parameters of our study. Therefore, in what follows we will express our results as a function of these parameters.

Several physical parameters entering in P_e and Π_v are known with a relatively small uncertainty. However, the diapir radius r_d and the silicate rock viscosity η can vary by several orders of magnitude. Therefore, the plausible range for P_e and Π_v values is large. Assuming that diapirs sink at Stokes velocity in the creeping flow regime $V_s \sim \Delta\rho_c g r_d^2/\eta$ in a solid proto-mantle, one can calculate P_e and Π_v for a plausible range of values of r_d and η. In that case using Eqs. (2) and (3), and assuming $\rho_0 \sim \Delta\rho_c = 4000$ kg m^{-3}, $P_e = \Delta\rho_c \rho_0 C_p g r_d^3/(\eta k)$ and $\Pi_v = r_d g/(\Delta T C_p)$.

We consider the viscosity range $\eta = [10^{13}$–$10^{22}]$ Pa s, in which the minimum value is the upper bound value corresponding to a partially molten proto-mantle (Karato and Murthy, 1997). The plausible range for r_d depends on the size distribution of accreting planetesimals and/or on the thickness of a surface magma ocean, for which significant

uncertainties remain. We therefore consider $r_d = [10^3$–$10^5]$ m, a range similar to that proposed by Karato and Murthy (1997).

Using $C_p = 1200$ J kg^{-1} K^{-1}, $\Delta T = 1000$ K the resulting ranges of variation for P_e and Π_v are shown in Fig. 1a and b, respectively. Π_v varies in the range $[0.01$–$1]$ while the range for P_e is $[10^{-3}$–$10^{13}]$.

Our numerical experiments covered the ranges $P_e = [10^{-3}$–$10^4]$ and Π_v $[0.01$–$10]$. Solving numerically the governing equations with very high values for P_e $(>10^6)$ is computationally prohibitive, as it requires higher resolution and smaller time steps. However, as we shall see later, in the limit of high P_e, diffusive heat transfer is negligible along sinking distances comparable to, or greater than, the radius of an Earth-sized planet.

The uncertainty in γ can also be large as the sensitivity of viscosity with temperature depends for instance on pressure, or on composition in major elements and minor elements (e.g., water), and can range from 10^5 to 10^{13} (Karato and Wu, 1993). Our numerical experiments cover γ values ranging from 1 to 10^6. Very large values of γ (i.e., $>10^6$) produce very sharp and large gradients in stresses and cause numerical difficulties.

Fig. 2 displays the nearly steady state dimensionless temperature field for a case with $P_e = 0.9$, $\Pi_v = 1$ and $\gamma = 1$. As observed in (Samuel and Tackley, 2008), viscous heating is mainly located at the diapir's "poles" in the silicate part and rapidly decreases away from the diapir. Part of this energy diffuses into the diapir while the remaining heat forms a halo around the diapir and a tail behind it. Fig. 3a displays the evolution of the diapir mean temperature T_d' as a function of its sinking distance d_s'. The solid lines correspond to numerical experiments only differing in the initial temperature of the sinking diapir T_{d0}'. The diapir temperature increases (black curve) or decreases (red and blue curves) with time, depending on T_{d0}' but always converges towards a specific value $T_{d\infty}'$. For a sinking distance
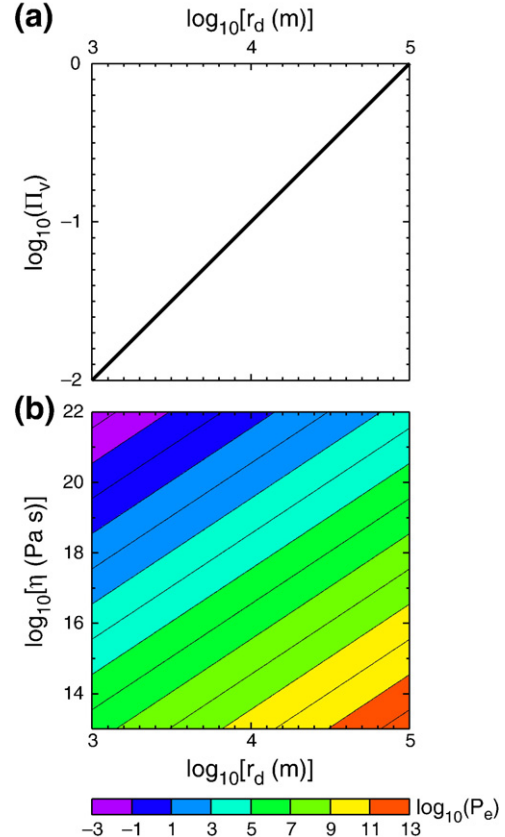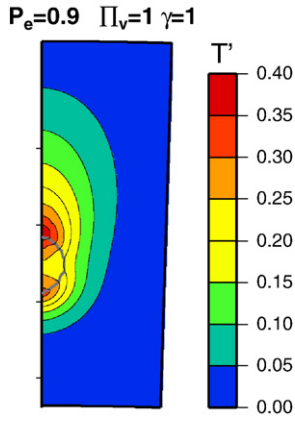

Fig. 1. (a) Π_v number as a function of a plausible range of diapir radius r_d. (b) Diapir Péclet number P_e as a function of a plausible range of diapir radius r_d and proto-mantle viscosities η.

Fig. 2. Results from the numerical experiments. Dimensionless potential excess temperature (close up view). The gray contour delineates the surface of the sinking diapir.

$d'_s > 6$ the temperature configuration for these three experiments is close or identical to that shown in Fig. 2.

We also observed this asymptotic behavior for cases with temperature dependent viscosity. The solid curves in Fig. 3b show the evolution of diapir mean temperature for two numerical experiments with $P_e = 0.4$, $\Pi_v = 1.2$ and $\gamma = 10^3$. Both curves converge toward the asymptotic value $T'_{d\infty}$ and the temperature field (not shown) is qualitatively similar to that displayed in Fig. 2.

We conducted various additional experiments with different values for P_e, Π_v and γ and we systematically find that after a
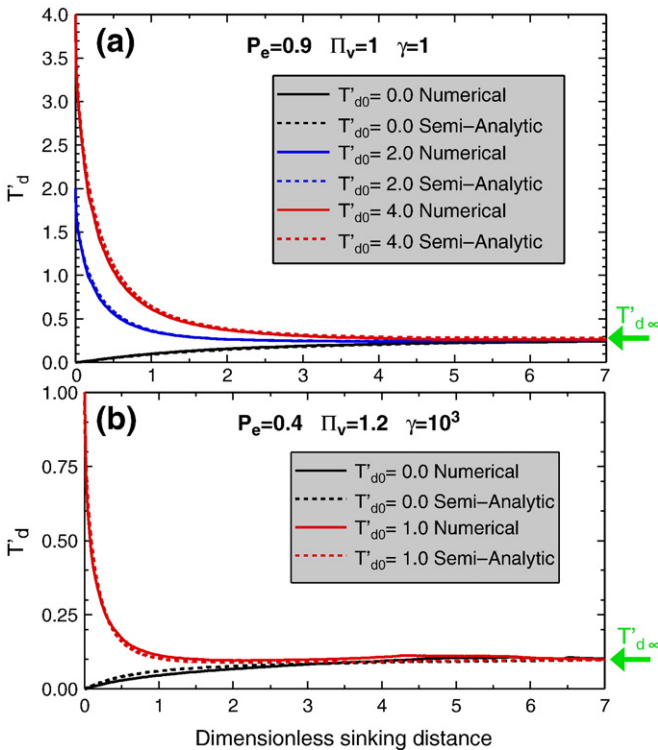
Fig. 3. Time evolution of the diapir average dimensionless potential excess temperature. (a) Comparison between three numerical and semi-analytical experiments. The green arrow indicates the asymptotic value $T'_{d\infty}$ calculated by solving Eq. (4) in the permanent regime. Each experiment has the following model parameters $P_e = 0.9$, $\Pi_v = 1$, $\gamma = 1$ and differ only by the initial temperature of the sinking diapir $T'_{d0} = (0, 2, 4)$. The green arrow indicates the asymptotic value of the diapir's mean temperature $T'_{d\infty}$ calculated by solving Eq. (5). (b) Same as in (a) for a different set of experiments. ($T'_{d0} = 0$ and $T'_{d0} = 1$), with $P_e = 0.4$, $\Pi_v = 1.2$, and $\gamma = 10^3$.

sufficiently long time T'_d evolves towards $T'_{d\infty}$. Therefore determining this asymptotic value is key to predicting the heat partitioning between a sinking metal diapir and its surroundings. Stress dependent rheology would affect the value of V_s, and therefore P_e, Π_v and $T'_{d\infty}$. However, the general behavior should remain similar to what we observed since even in that case the diapir reaches a terminal sinking velocity (Samuel and Tackley, 2008).

2.2. Semi-analytic model for determining $T'_{d\infty}$

To better characterize the thermal evolution of sinking diapirs, we use the model developed in (Samuel and Tackley, 2008), whose simplifying assumptions are: (i) adiabatic heating and thermal density differences are negligible, (ii) the diapir remains spherical and its viscosity is small compared to that of the surroundings, (iii) velocities are approximated by the analytic solution of Hadamard (1911) and (Rybczynski, 1911) (see also (Batchelor, 1967)), in spherical axisymmetric coordinates (r, θ) centered on the diapir. This is reasonable given the relatively low diapir Reynolds numbers considered in our experiments. Under these assumptions, the remaining equation to solve is conservation of energy, which simplifies to:

$$\frac{\partial T'}{\partial t'} + \mathbf{U}'.\nabla T' = \frac{1}{P_e}\nabla^2 T' + \Pi_v \phi'_v. \tag{4}$$

An additional advantage in using the semi-analytic model, is that it allows one to consider much larger values of γ than what can be achieved with the full numerical experiments. We tested the ability of the semi-analytic model (i.e., Eq. (4) solved by finite differences) to capture the essential physics and to reproduce the numerical experiments by performing runs with the same parameters as those used in the numerical experiments. The results displayed in Fig. 3a–b show that the semi-analytic model reproduces well the numerical experiments, even for temperature dependent viscosity. Additional comparisons were performed for various $P_e = [10^{-1}–10^4]$, $\Pi_v = [0.01–10]$ and $\gamma = [1–10^6]$ and we found a good agreement between the semi-analytic model and the numerical experiments. This shows that the assumptions made for the semi-analytic model are reasonable. As mentioned in the previous section, very high γ values ($>10^6$) could not be considered for the numerical experiments. Therefore, the comparison between numerical experiments and semi-analytical model could not be performed for the range $\gamma = [10^7–10^{13}]$. However, as shown in (Samuel and Tackley, 2008), for $P_e > 1$, the low viscosity zone due to the temperature increase is confined to a thin layer around the diapir and its influence on the diapir sinking velocity and the whole dynamics is very weakly influenced by higher values of γ. Higher values of γ would tend to lead to larger sinking velocities and therefore larger values of P_e and Π_v. Nevertheless, the whole dynamics should remain the same. Therefore, we are confident that the agreement between the numerical experiments and the semi-analytical model would remain good for greater values of γ.

The relative simplicity of the semi-analytic model allows for a more intensive exploration of the parameter space P_e, Π_v and γ at a more affordable computational cost. In addition, by solving Eq. (4) to steady state we can determine $T'_{d\infty}(P_e, \Pi_v, \gamma)$:

$$\mathbf{U}'.\nabla T'_{d_\infty} = \frac{1}{P_e}\nabla^2 T'_{d_\infty} + \Pi_v \phi'_v. \tag{5}$$

Unfortunately, the temperature dependence of viscosity introduces a non-linearity in the viscous heating term in Eq. (5), which is difficult to treat analytically. Instead, we solve numerically for Eq. (5) using a fast direct solver (superLU, (Demmel et al., 1999)) on a finite difference grid. As time stepping is no longer involved in Eq. (5), the computational expenses are greatly reduced. This enables us to calculate $T'_{d\infty}$ for broad ranges of variations for $P_e = [10^1–10^6]$, $\Pi_v =$

$[10^{-3}$–$10^6]$, and for $\gamma = [10^3$–$10^{13}]$. For this explored range of parameters, we express $T'_{d\infty}$ as the sum of two contributions:

$$T'_{d\infty} = a_0(P_e, \gamma) + a_1(\Pi_v, \gamma), \tag{6}$$

where $a_0(P_e, \gamma) = 0.13/[0.043(1 + 0.52\ln\gamma) + P_e^{-0.5}]$ and $a_1(\Pi_v, \gamma) = 910^{-3}\ln\Pi_v/(1 - \gamma^{-0.01})$. Similar to (Samuel and Bercovici, 2006) The empirical functions $a_0(P_e, \gamma)$ and $a_1(\Pi_v, \gamma)$ were determined by collapsing successively the curves $T'_{d\infty}$ calculated as a function of P_e, Π_v and γ into the empirical expression (6), following the approach described in (Ribe, 1996). Comparisons between the approximate values of $T'_{d\infty}$ obtained using Eq. (6), and the solutions of Eq. (5) are displayed in Fig. 4 for various values of P_e, Π_v and γ. Eq. (6) has an uncertainty of less than 10% and neglects significantly low values of $T'_{d\infty}$ (i.e.,<0.09).

2.3. Analytic model for the diapir thermal evolution

Despite its relative simplicity, the semi-analytical diapir sinking model remains computationally expensive due to the time dependence. This prohibits the use of Eq. (4) for investigating core formation heat partitioning with thousands or millions of sinking diapirs. Therefore, in this section we further simplify the semi-analytic diapir sinking model to an analytic expression. As sketched in Fig. 5, the thermal state of the sinking diapir of volume $V_d = 4/3\pi r_d^3$ is now represented only by its mean temperature T_d. The diapir exchanges heat with an intermediate shell of constant volume fV_d and of homogeneous temperature T_i where viscous heating occurs. The intermediate region is surrounded by an outer shell of homogeneous potential temperature $T_0 = 0$ where viscous heating is negligible. Heat exchange between these different regions occurs though boundary layers formed in the silicate proto-mantle. As for the numerical experiments and the semi-analytical model, the physical parameters for the diapir and the surrounding proto-mantle are identical, except for viscosity, which is assumed to be negligible in the diapir.

The conservation of energy for the sinking diapir (neglecting viscous heating within the diapir due to its very low viscosity) is:

$$\frac{d}{dt}\left(\frac{4\pi r_d^3}{3}C_p(\rho_0 + \Delta\rho_c)T_d\right) = -4\pi r_d^2\frac{k}{\delta}(T_d - T_i) \tag{7}$$

with $\delta = \sqrt{2r_d k/(\rho_0 C_p V_s)}$ the thickness of the thermal boundary layer across which heat diffusion occurs.

The conservation of energy for the intermediate region is:

$$\frac{d}{dt}\left(f\frac{4\pi r_d^3}{3}C_p\rho_0 T\right) = F_i + V_d\phi_v, \tag{8}$$
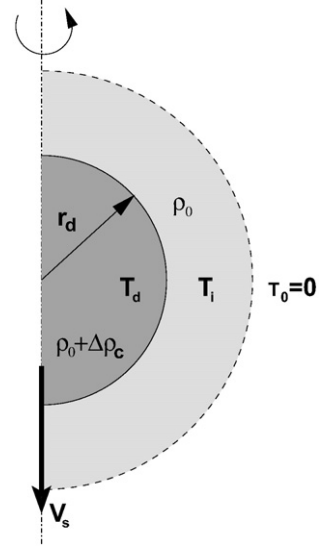
Fig. 5. Schematic view of the sphere-shell analytic model. The sinking metal diapir is represented by a sphere of homogeneous temperature T_d. It is surrounded by an intermediate shell region composed of lighter material (light gray area) of homogeneous temperature T_i where viscous heating is important. See text for further definition of the symbols.

where ϕ_v is the dissipation function F_i expresses the diffusive heat flux towards both the diapir and the outer shell regions, and is approximated by $-k4\pi r_d^2(2T_i - T_d)/\delta$. As confirmed by the results of our numerical and semi-analytical experiments, the time dependence of F_i is weak because T_i and T_d are coupled. We therefore make the reasonable assumption that $dF_i/dt \cong 0$ over small time intervals, and using Eq. (8) we calculate the time averaged value of T_i over a sinking time $2rd/V_s$, yielding:

$$T_i = \frac{C_i}{1 + 2C_i}(T_d + \Delta T_i), \tag{9}$$

where $C_i = 6k/(\rho_0 C_p f\delta V_s)$ and ΔT_i, is the average temperature increase in the intermediate region due to viscous heating. With our Lagrangian frame of reference located at the center of the sinking diapir, the material present in the intermediate shell region, in contact with the sinking diapir, is continuously replaced by new material that has not been previously heated (i.e., with a temperature T_0). Therefore, the local increase of temperature in the intermediate region due to viscous heating is bounded, and we assume that ΔT_i is constant with time. We express ΔT_i by assuming that along a sinking distance $2r_d$, all the gravitational energy released: $\Delta E_p = V_d \Delta\rho_c g2r_d$, is converted into heat in the intermediate region, $\Delta E_i = fV_d \rho_0 C_p \Delta T_i$. This is consistent with conservation of energy and yields an expression for the average temperature increase due to viscous heating in the intermediate shell:

$$\Delta T_i = \frac{2\Delta\rho_c gr_d}{f\rho_0 C_p}. \tag{10}$$

Substituting Eq. (9) into Eq. (7) and integrating yields, upon non-dimensionalization by the scales used in section 2.1:

$$T'_d = \Pi_v^* + (T'_{d0} - \Pi_v^*)\exp\left(-\frac{1}{P_e}t'\right), \tag{11}$$

where P_e^* is a modified Péclet number:

$$P_e^* = \frac{\sqrt{2}(\rho_0 + \Delta\rho_c)}{3\rho_0}\frac{1 + 2C_i}{1 + C_i}P_e^{1/2}. \tag{12}$$
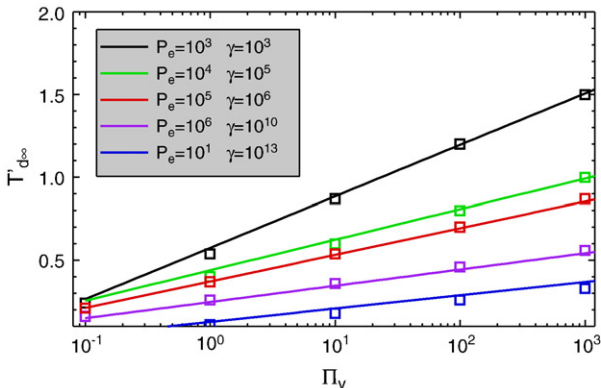

Fig. 4. Comparison between the results for $T'_{d\infty}$ calculated by solving Eq. (5) (symbols) and the empirical Eq. (6) (solid curves) for various values of P_e, Π_v and γ.

Note that for core formation in terrestrial planets, $\rho_0 \sim \Delta\rho_c$ and therefore $P_e^* \sim P_e^{1/2}$ for any value of C_i. Similarly to Π_v, the second dimensionless number expresses the efficiency of viscous heating

$$\Pi_v^* = \frac{\Delta T_i}{\Delta T} \frac{1}{1 + C_i}. \tag{13}$$

Π_v^* also corresponds to $T_{d\infty}'$, as $\lim_{t \to \infty} T_d' = \Pi_v^*$, and can therefore be determined using Eq. (6).

All the parameters in Eqs. (11), (12) and (13) are known, with the exception of f, which is needed to determine P_e^* accurately. With the knowledge of $T_{d\infty}'$, and using Eqs. (10), (11) and (13) $f = 2r_d g \Delta\rho_c / [\rho_0 C_p \Delta T_{d\infty}(1 + C_i)]$. Note that the simplifying assumptions we made for the analytic model (e.g., averaging spatially varying quantities such as T_i, T_d, δ) lead to the appearance of scaling constants. These constants do not appear explicitly in the analytical model, but are contained in the parameter f, which is adjusted using the semi-analytical model (i.e., $T_{d\infty}'$, the solution of Eq. (5)).

We successfully tested the ability of Eq. (11) to reproduce the thermal evolution of the semi-analytic model (Eq. (4)) for various values of P_e, of Π_v and γ. For instance, Fig. 6a displays the time evolution of the average diapir temperature for the semi-analytic model (solid curves) and the analytic model (dashed curves), for $P_e = 10$, $\Pi_v = 100$ and $\gamma = 1000$. Two different initial diapir temperatures are considered $T_{d0}' = 0$ (black curves) and $T_{d0}' = 4$ (red curves). In both cases, the agreement between semi-analytic and analytic models is good. We carried similar successful comparisons between the analytic model and the numerical experiments (e.g., for $P_e = 32$, $\Pi_v = 0.3$ and $\gamma = 1000$, see Fig. 6b), which show that Eq. (11) captures the thermal evolution of a sinking diapir.
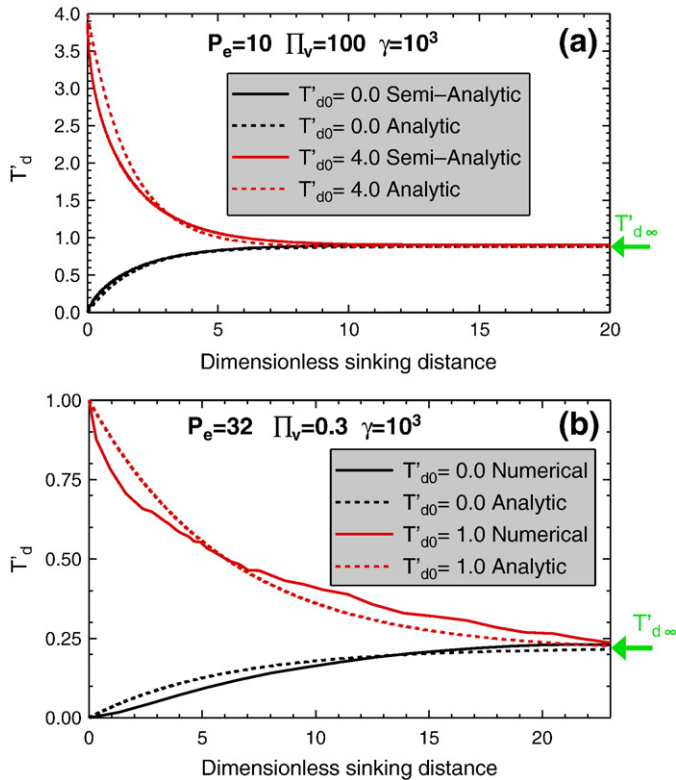

Fig. 6. (a) Comparison between the semi-analytic and analytic models. Time evolution of the diapir average dimensionless potential excess temperature for two experiments with identical parameters, but with two different initial temperatures T_{d0}'. The green arrow indicates the asymptotic value $T_{d\infty}'$ calculated by solving Eq. (5). (b) same as (a), for a different set of model parameters.

3. Application to core formation on Mars and the Earth

Here we illustrate a possible application of the scaling laws we derived to determine the total gravitational heat partitioning due to core formation first in a Mars-sized planet (i.e., with a planet radius $R_p = 3500$ km and a final core radius of 1600 km), then in an Earth-sized planet (i.e., with a planet radius $R_p = 6400$ km and a final core radius of 3500 km). For simplicity, we restrict our example to a crudely simplified scenario: The undifferentiated planet has an initial potential temperature profile set to $T_0 = 1300$ K with a surface thermal boundary layer. Initially n_{d0} iron diapirs of equal size (r_{d0}), in thermal equilibrium with the silicate rocks are randomly located in the upper 1000 km of the planet (Fig. 7a). Each diapir is represented by its location (r_d^p, θ_d, ϕ_d) and its radius r_d. Their total volume corresponds to the present-day Mars' core. The only heat source we consider is gravitational heating and the only mechanisms of heat transfer we consider are advection (via the sinking of the diapirs) and thermal diffusion between each diapir and their surrounding silicate mantle. Gravity is a function of the radial location r_p as $g = (4/3)\pi G \bar{\rho} r_p$ with $\bar{\rho}$ the average density of the planet, and G the gravitational constant. Similar to Senshu et al., (2002), each diapir sinks at the Stokes velocity $V_s(r_d^p, \theta_d, \phi_d)$ of a frictionless sphere (Hadamard, 1911; Rybczynski, 1911). The viscosity used to calculate $V_s(r_d^p, \theta_d, \phi_d)$ depends on temperature as: $\eta = \eta_0 \exp[-\ln(\gamma)(T(r) - T_0)]$, with $\eta_0 = 10^{21}$ Pa s and $\gamma = 10^{10}$. Other model parameters are: $\rho_0 = \Delta\rho_c = 4000$ kg m^{-3}, $k = 3$ W m^{-1} K^{-1}, $C_p = 1200$ J kg^{-1} K^{-1}, $\Delta T = 1000$ K.

The planet radius is discretized into 200 to 1000 points with a spacing Δr and we consider a time step that satisfies a Courant criteria (i.e., $\Delta t < MIN(\Delta r / V_s)$ over the whole domain and for all diapirs). At every time iteration each diapir position is updated. We assume diapir merging when the distance between two diapirs is smaller than the diameter of the larger one. Upon merging, the position of the newly formed diapir is determined by simple weighted average and its thermal energy is the sum of the merging diapirs. We follow the thermal evolution of the planet until complete core formation is achieved (Fig. 7b). We find that 99% of the core is formed within a few millions of years or less depending on the initial size of the iron diapirs, which is consistent with geochemical considerations (Kleine et al., 2004a,b).

Given the choice of physical parameters, the initial diapirs' Péclet numbers range from 10^1 to 10^5 depending on the value of n_{d0} (see Fig. 1b). However as they sink, each diapir's Péclet number may change, due to changes in viscosity and to diapir merging, and may exceed 10^6 (see Fig. 1b), for which Eq. (6) may not give accurate results. However, one can show that in that case diffusive heat transfer is so inefficient that the diapir temperature remains essentially constant until the end of core formation. This can be seen by estimating the sinking distance d_β,
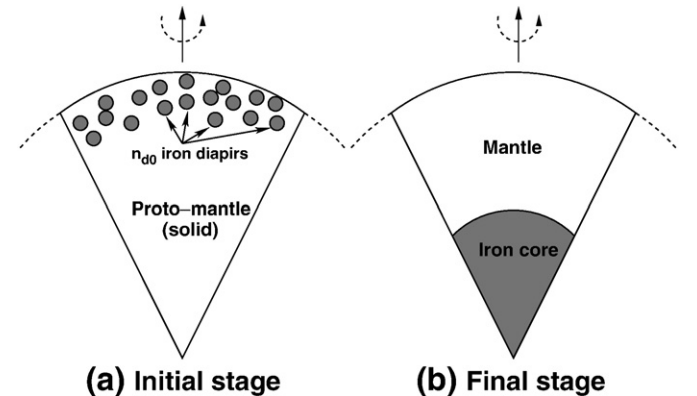
Fig. 7. Schematic representation of the initial (a) and final stages (b) of the core formation scenario considered in section (3).

necessary for a diapir (with zero initial temperature) to reach a fraction β of its asymptotic value $T_{d\infty}$. Using Eq. (11): $d_\beta = -r_d P_e^* \ln(1-\beta)$. Then using $P_e^* \sim P_e^{1/2}$ (see section 2.3 and Eq. (12)), one finds:

$$d_\beta \cong -r_d P_e^{1/2} \ln(1-\beta). \qquad (14)$$

Using Eq. (14) with a relatively small value for β, say 0.1, the dimensional sinking distance d_β necessary for a diapir to reach $\beta = 10\%$ of its asymptotic temperature $T_{d\infty}$ is $d_\beta \cong 0.1 r_d P_e^{1/2}$. Therefore for $P_e > 10^6$, $d_\beta > 10 r_d$. Given the values of n_{d0} considered, the initial value of r_d is 10^4–10^5 km and tends to increase with time due to diapir merging and the decrease of viscosity with increasing temperature. This corresponds to $d_\beta > (1$–$10)R_p$. Therefore, we can reasonably consider that diapirs with $P_e > 10^6$ have essentially a constant temperature. In other words, the thermal energy produced by viscous heating around diapirs with $P_e > 10^6$ remains in the silicate proto-mantle.

Although gravity varies with depth we use Eq. (11) that assumes constant gravitational acceleration g. However, the CFL criteria we consider implies that Eq. (11) is used over small time intervals Δt (or small sinking distances) during which the assumption that g is constant remains reasonable.

3.1. Influence of the treatment of heat partitioning

Previous models of core formation via negative diapirism in terrestrial planets have assumed that heat partitioning between the sinking diapirs and their surroundings was fixed to a constant value (Senshu et al., 2002). In order to test the validity of this hypothesis we assume that the amount of gravitational heat that is transferred to each diapir, F_d^h, is either fixed to an arbitrary value: 0%, 50% and 100%, or is determined using Eq. (11) (dotted blue curve). Fig. 8a displays the potential temperature profiles of the planet after complete core formation with $n_{d0} = 10^4$.

The treatment of gravitational heat partitioning drastically affects the early thermal profile of the planet. Only the fixed $F_d^h = 25\%$ curve compares well with the more realistic dotted blue profile (determined using Eq. (11)). However, as illustrated in the next section, this value can be strongly influenced by parameters such as the size and the size distribution of the metal diapirs, or the accretional history of the growing planet (Kokubo and Ida, 1996). Therefore, assuming a constant and arbitrary value for F_d^h most likely leads to incorrect predictions for the thermal state of a young planet.

3.2. Influence of the initial size of iron diapir on core formation heat partitioning

We now use exclusively our analytical model (Eq. (11)) to determine the core formation heat partitioning for a Mars-sized planet, and we varied n_{d0} between 1000 and 610^6 (corresponding $r_{d0} \cong 20$–160 km). Fig. 8b illustrates the influence of r_{d0} (or n_{d0}) on the core–mantle partitioning of the heat released during core formation. This partitioning can be represented by F_{Si}^h, the ratio of the total gravitational energy released during core formation to the total increase of thermal energy in the silicate mantle. For high values of n_{d0} (i.e., small initial size of iron diapirs r_{d0}) F_{Si}^h decreases. This is mainly due to the fact that as the diapir size increases their individual P_e (or P_e^*) increases. Consequently, larger diapirs do not have time to thermally equilibrate with the surrounding silicate material where viscous heating takes place (see section 1 and Eq. (14)). Larger n_{d0} values (smaller initial diapir sizes) lead to lower Péclet numbers allowing for thermal equilibration between the diapirs and the silicate mantle (Fig. 8b). Note that even diapirs with modest viscous heat production (low Π_v) can transfer significant amounts of heat to the core by traveling through hotter silicate regions (left for instance by previous diapirs).
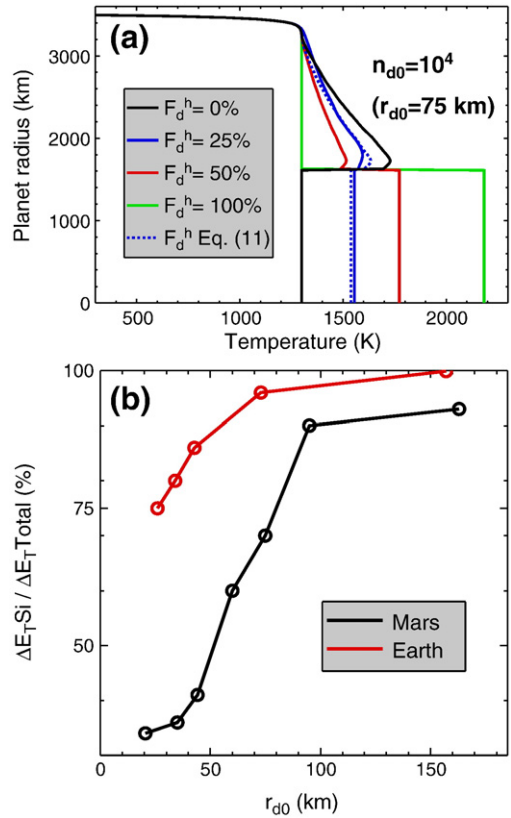
Fig. 8. Results from the differentiation model after complete formation of a metallic core by negative diapirism. (a) Potential temperature profiles. Partitioning of gravitational heating, F_h, between the sinking iron diapir and the surrounding silicate material is either assumed to be fixed to a constant value, or is determined using Eq. (11). (b) Influence of the initial radius of iron diapirs, r_{d0}, on the total partitioning of core formation heating.

We iterate similar experiments, but for a larger, Earth-sized planet (with a planet radius $R_p = 6400$ km and a final core radius of 3500 km). The trend for the dependence of heat partitioning F_{Si}^h as a function of the initial diapir size remains similar to what was shown for Mars-sized cases in Fig. 8b. However, we find that F_{Si}^h values are significantly higher. Indeed, for an Earth-sized planet, the diapirs' Péclet numbers Pe are larger due to the higher gravity and the more frequent occurrence of diapir merging. Thus, even if the sinking distance of the diapir is extended and viscous heating is more important, the heat transfer between the sinking diapir and the surrounding hot proto-mantle is even more reduced. This results in an even hotter lowermost mantle than we observe for a Mars-sized planet.

4. Discussion

Our results have strong implications for our understanding of the initial stages and the long term thermo-chemical evolution of terrestrial planets. Indeed, as suggested by Fig. 8a–b large diapir size will leave the planet's metallic core relatively cold. This would tend to prevent a sustainable planetary dynamo, as in the case of Mars (Acuña et al., 1998). Conversely, small diapir sizes would lead to a hotter core and a colder mantle. This core super heat would then favor the presence of a sustainable dynamo, as on Earth. In addition, core formation would leave the bottom of the silicate mantle significantly hotter than its upper part (Fig. 8a), which could generate a basal magma ocean (Labrosse et al., 2007).

Clearly, these questions need to be addressed systematically, in a more realistic setting than our simple differentiation model by including internal heating, radiation, convection, or impact heating, (Monteux et al., 2007; Sasaki and Nakazawa, 1986; Senshu et al., 2002), or a more

realistic size distribution and timing for generation of the metal diapirs based for instance on N-body simulations, (Nimmo and Agnor, 2006). In particular, impact heating certainly plays an essential role in the early thermal state of a young planet and initial core super heat. As pointed out by Ricard et al., (2009) the amount of energy delivered by impact heating is comparable to that provided by core formation in an Earth-sized planet. As a consequence, iron diapirs with high P_e numbers would tend to deliver to the core relatively small amounts of viscous heating but relatively large amounts of impact heating, and vice-versa. For these reasons, the values of heat partitioning mentioned in this section are certainly not definitive. Given the substantial uncertainties tied to these processes, a systematic approach is highly desirable for future research.

However, the results displayed in Fig. 8a–b clearly demonstrate that gravitational heat partitioning during core formation has a first order impact on the initial thermal state of a terrestrial planet. Furthermore, it cannot be treated in any arbitrary fashion and we recommend the use of Eq. (11), which can be straightforwardly incorporated into thermo-chemical evolution models of growing terrestrial planets (Sasaki and Nakazawa, 1986; Senshu et al., 2002).

5. Conclusions

We performed numerical experiments to investigate the gravitational heat partitioning between metal diapirs sinking through a lighter proto-mantle, with a rheology that strongly depends on temperature and composition. All our experiments show an asymptotic behavior of the diapir mean temperature towards $T_{d\infty}$ that we determined empirically. This value is independent of the initial temperature of the diapir and depends on the diapir Péclet Number Pe, on the importance of viscous heating Π_v, and on the rheology.

We developed a simple analytical model for the thermal evolution of sinking metal diapirs that closely reproduces our numerical results.

We have applied these scaling laws in a simplified core formation model to determine the core formation heat partitioning in Mars and Earth sized planets.

We show that the partitioning of core formation heating during negative diapirism depends strongly on the size distribution of the iron diapirs. A large number of small sinking iron diapirs favors metal–silicate heat exchange and leads to a relatively hot core, which allows a sustainable dynamo, as on Earth. A small number of large diapirs has the opposite effect and could correspond to a Mars-like planet with an early dynamo that is no longer active.

In all cases, negative diapirism tends to leave the lowermost mantle significantly hotter than its upper part, which could trigger large amounts of melting in the early deep mantle.

While we show that gravitational heat partitioning during core formation cannot be treated in any arbitrary fashion, our analytical model can easily be incorporated in thermo-chemical evolution models of growing terrestrial planets.

Acknowledgements

References

Acuña, M.H., Connerney, J.P., Wasilewski, P., Lin, R.P., Anderson, K.A., Carlson, C.W., McFadden, J., Curtis, D.W., Mitchell, D., Reme, H., Mazelle, C., Sauvaud, J.A., dUston, C., Cros, A., Medale, J.L., Bauer, S.J., Cloutier, P., Mayhew, M., Winterhalter, D., Ness, N.F., 1998. Magnetic field and plasma observations at Mars: initial results of the Mars global surveyor mission. Science 279, 1676–1680.
Batchelor, G.K., 1967. An Introduction to Fluid Dynamics. Cambridge University Press, Cambridge.
Demmel, J.W., Eisenstat, S.C., Gilbert, J.R., Li, X.S., Liu, J.W., 1999. A supernodal approach to sparse partial pivoting. SIAM J. Matrix. Anal. Appl. 20, 720–755.
Golabek, G.J., Schmeling, H., Tackley, P.J., 2008. Earth's core formation aided by flow channelling instabilities induced by iron diapirs. Earth Planet. Sci. Lett. 271, 24–33.
Hadamard, J., 1911. Mouvement permanent lent d'une sphère liquide et visqueuse dans un liquide visqueux. C. R. Acad. Sci. 152, 1735–1738.
Karato, S.-I., Wu, P., 1993. Rheology of the upper mantle: a synthesis. Science 260, 771–778.
Karato, S.-I., Murthy, R.V., 1997. Core formation and chemical equilibrium in the Earth — I. Physical considerations. Phys. Earth. Pl. Int. 100, 61–79.
Kleine, T., Mezger, K., Münker, C., Palme, H., Bischoff, A., 2004a. ^{182}Hf–^{182}W isotope systematics of chondrites, eucrites, and martian meteorites: chronology of core formation and early mantle differentiation in Vesta and Mars. Geochim. Cosmochim. Acta 68, 2935–2946.
Kleine, T., Mezger, K., Palme, H., Münker, C., 2004b. The W isotope evolution of the bulk silicate Earth: constraints on the timing and mechanisms of core formation and accretion. Earth Planet. Sci. Lett. 228, 109–123.
Kokubo, E., Ida, S., 1996. On runaway growth of planetesimals. Icarus 123, 180–191.
Labrosse, S., Hernlund, J.W., Coltice, N., 2007. A crystallizing dense magma ocean at the base of the Earth's mantle. Nature 450, 866–869.
Monteux, J., Coltice, N., Dubuffet, F., Ricard, Y., 2007. Thermo-mechanical adjustment after impacts during planetary growth. Geophys. Res. Lett 34, l24201. doi:10.1029/2007GL031635.
Monteux, J., Ricard, Y., Coltice, N., Dubuffet, F., Ulvrova, M., 2009. A model of metal–silicate separation on growing planets. Earth Planet. Sci. Lett. 287 (3–4), 353–362.
Nimmo, F., Agnor, C.B., 2006. Isotopic outcomes of N-body accretion simulations: constraints on equilibration processes during large impacts from Hf/W observations. Earth Planet. Sci. Lett. 243, 26–43.
Olson, P., Weeraratne, D.S., 2008. Experiments on metal–silicate plume and core formation. Phils. Trans. R. Soc. London, Ser. A 366, 4253–4271.
Ribe, N.M., 1996. The dymancs of plume–ridge interaction 2. Off-ridge plumes. J. Geophys. Res. 96, 16195–16204.
Ricard, Y., Sramek, O., Dubuffet, F., 2009. A multi-phase model of runaway core–mantle segregation in planetary embryos. Earth Planet. Sci. Lett. 284, 144–150.
Rubie, D.C., Nimmo, F., Melosh, H.J., 2007. Formation or Earth's core. In: Schubert, G., Stevenson, D.J. (Eds.), Treatise on Geophysics, vol. 9. Elsevier, pp. 51–90.
Rybczynski, W., 1911. Über die fortschreitende bewegung einer flüssigen Kugel in einen Medium. Bull. Acad. Sci. Cracovie 1, 40–46.
Samuel, H., Bercovici, D., 2006. Oscillating and stagnating plumes in the Earth's lower mantle. Earth Planet. Sci. Lett. 248, 90–105.
Samuel, H., Tackley, P.J., 2008. Dynamics of core formation and equilibration by negative diapirism. Geochem. Geophys. Geosyst. 9. doi:10.1029/2007GC001896.
Sasaki, S., Nakazawa, K., 1986. Metal–silicate fractionation in the growing Earth: energy source for the terrestrial magma ocean. J. Geophys. Res. 91, 9231–9238.
Senshu, H., Kuramoto, K., Matsui, T., 2002. Thermal evolution of a growing Mars. J. Geophys. Res. 107. doi:10.1029/2001JE001819.
Solomon, S.C., 1979. Formation, history and energetics of cores in the terrestrial planets. Phys. Earth. Pl. Int. 19, 168–182.
Stevenson, D.J., 1981. Models of the Earth's core. Science 214, 611–619.
Tackley, P.J., 2008. Modelling compressible mantle convection with large viscosity contrasts in a three-dimensional spherical shell using the yin-yang grid. Phys. Earth. Pl. Int. 171, 7–18.
Tonks, B.W., Melosh, J.H., 1992. Core formation by giant impacts. Icarus 100, 326–346.